

General Disclaimer

One or more of the Following Statements may affect this Document

- This document has been reproduced from the best copy furnished by the organizational source. It is being released in the interest of making available as much information as possible.
- This document may contain data, which exceeds the sheet parameters. It was furnished in this condition by the organizational source and is the best copy available.
- This document may contain tone-on-tone or color graphs, charts and/or pictures, which have been reproduced in black and white.
- This document is paginated as submitted by the original source.
- Portions of this document are not fully legible due to the historical nature of some of the material. However, it is the best reproduction available from the original submission.

**NASA TECHNICAL
MEMORANDUM**

NASA TM X-73598

NASA TM X-73598

(NASA-TM-X-73598) OPTICAL PROPERTIES OF ION
BEAM TEXTURED METALS (NASA) 20 p HC A02/MF
A01 CSCL 11F

N77-18251

Unclas
G3/26 17200

OPTICAL PROPERTIES OF ION BEAM TEXTURED METALS

by W. R. Hudson, A. J. Weigand, and M. J. Mirtich
Lewis Research Center
Cleveland, Ohio 44135



TECHNICAL PAPER to be presented at the
Sixth Annual Symposium on Applied Vacuum Science and Technology
sponsored by the American Vacuum Society
Tampa, Florida, February 14-16, 1977

OPTICAL PROPERTIES OF ION BEAM TEXTURED METALS

by W. R. Hudson, A. J. Weigand, and M. J. Mirtich

Lewis Research Center

ABSTRACT

Copper, silicon, aluminum, titanium and 316 stainless steel were textured by 1060 eV xenon ions from an 8-cm diameter electron bombardment ion source. Simultaneously sputter-deposited tantalum was used to facilitate the development of the surface microstructure.

Scanning electron microscopy of the ion textured surfaces revealed two types of microstructure. Copper, silicon, and aluminum developed a cone structure with an average peak-to-peak distance ranging from 1 μm for silicon to 6 μm for aluminum. Titanium and 316 stainless steel developed a serpentine ridge structure. The average peak-to-peak distance for both of these materials was 0.5 μm . Spectral reflectance was measured using an integrating sphere and a holraum reflectometer. Total reflectance for air mass 0 and 2, solar absorptance, α_S , and total emittance, ϵ_T , normalized for a 425 K black body were calculated from the reflectance measurements. All materials had solar absorptances between 0.93 (stainless steel) and 0.97 (silicon and aluminum). Total emittance values of 0.75, 0.80, and 0.85 for Si, Al, and Cu, respectively, resulted in α_S/ϵ_T of approximately 1.2. Titanium ($\epsilon_T = 0.37$) and 316 stainless steel ($\epsilon_T = 0.32$) had α_S/ϵ_T values of 2.6 and 2.9, respectively. The optical properties for all materials investigated compare favorably with coatings presently employed for solar heating applications.

INTRODUCTION

The increased awareness of the nation's future energy requirements has created considerable interest in the utilization of solar energy. The ultimate contribution that solar energy can make to the nation's energy needs depends on whether the conversion of solar energy into usable energy can be made economically competitive with other energy sources. One of the methods of utilizing solar energy is through solar-thermal collection systems. The costs of a solar-thermal collection system depend on system component production costs and the efficiency of energy collection and retention. The energy collection efficiency depends on the optical properties of the solar collectors. It has been estimated that production costs for ion textured surfaces would range from \$550./m² (\sim \$50./ft²) for special items to several tens of dollars/m² (\sim several dollars/ft²) for mass produced items.

The general principles and applications of selective solar coatings has recently been discussed by Jurisson, Peterson and Mar (ref. 1). They discuss vacuum-deposited coatings, electroplated coatings, paint-

type coatings and chemically etched coatings as means of achieving selective solar surfaces. Another way of modifying the optical properties of surfaces is by ion beam texturing. Some preliminary research on copper surfaces has been done in this area by Berg and Kominiak (ref. 2). The first extensive study of the ion beam texturing process was performed by Wehner and Hajicek (ref. 3). More recently the texturing process has been studied for thirty elements by Hudson (ref. 4). Ion beam texturing is the creation of a microscopic surface roughness by sputter etching the target while depositing a low sputtering yield seed material onto the target surface.

Five materials [316 stainless steel (SS), titanium (Ti), aluminum (Al), copper (Cu), and silicon (Si)] of general interest for solar energy applications have been textured. Scanning electron photomicrographs have been taken of each surface to characterize the resulting morphology. Measurements of spectral reflectance (specular and diffuse) between 0.33 and 16 μm have been made for each material. Solar absorptance (α_s) for air mass 0 and 2 and total emittance normalized for a 425 K blackbody were calculated from the data. Graphs showing spectral reflectance for each ion textured material are presented. Equilibrium temperature measurements of a collector surface in space and terrestrial environments were calculated for each material.

ION BEAM TEXTURING PROCESS

An eight-centimeter diameter, xenon ion source (fig. 1) was used in the texturing process. The ion source design is an outgrowth of technology previously developed for electron bombardment ion thrusters. The ion source uses hollow cathodes (ref. 5) as both the main cathode and the neutralizer. The magnetic circuit is a cusped field geometry (ref. 6), with permanent rod magnets around the perimeter of the discharge chamber.

Beam extraction is accomplished by a dished, two grid ion optics system (ref. 5). The vacuum facility maintained a vacuum of 1×10^{-5} torr during ion source operation. The facility was sufficiently large to minimize backspattered facility material from contaminating the experiments.

The ion source is capable of operating at beam energies between 500 and 2000 eV. The beam current is adjustable between 10 milliamperes and 200 milliamperes. However, for the data reported herein the ion source was operated at a beam energy of 1000 eV and a beam current of 100 milliamperes. The samples were positioned 10 cm from the ion source at the center of the beam. The current density at this location is 2.0 ma/cm^2 .

Figure 2 shows the arrangement of the source, seed material, and target used in the ion beam texturing process. A 2.4 cm diameter sample to be textured (target) was positioned so that the ion source axis was normal to its surface. The seed material was mounted on a separate support and oriented at a forty-five degree angle with respect to the source axis. The seed material was located within the ion beam envelope very close to, but not touching, the target. The ion beam simultaneously sputtered both the target and the seed material. The process results in a microscopic surface texture on the target. Targets as large as 12 cm could be textured using the 8-cm diameter ion source.

The physical mechanism of the texturing process is thought to be the result of an agglomeration of the low sputtering yield seed material into microscopic regions on the surface of the target. The target regions beneath the islands of seed material are preferentially protected during sputtering and a texture develops. It is thought that as the process continues the seed material islands are replenished by thermally activated surface migration (ref. 3).

SPECTRAL REFLECTANCE MEASUREMENTS

The apparatus used for spectral reflectance measurements between 0.33 and 2.30 μm is shown in figure 3. The system consists of a tungsten strip filament lamp, monochromator, transfer optics, and an integrating sphere. The monochromator is a single-beam, double-pass, lithium fluoride prism instrument with an adjustable slit width. The 20-cm diameter integrating sphere (ref. 7) has an electrostatically smoked magnesium oxide coating approximately 2-mm thick. The sample is mounted on a holder such that it is in the center of the sphere. The sample is positioned so that incident light strikes the sample 15 degrees from the sample normal. Two radiometers are located on the sphere wall. A 1P28 photomultiplier tube is used for the wavelength region 0.33 to 0.665 μm . A lead sulfide detector covers the range from 0.63 to 2.16 μm . A lock-in voltmeter, phased with a 13 cps mechanical chopper within the monochromator, is used to record the detector output signal. The total solar reflectance at air mass zero, ρ_{S_0} , is defined as the solar energy (specular and diffuse components) reflected by a surface divided by the total energy incident upon the surface. Mathematically this relation is

$$\rho_{S_0} = \frac{\int_0^{\infty} \rho(\lambda) J_{S_0}(\lambda) d\lambda}{\int_0^{\infty} J_{S_0}(\lambda) d\lambda} \quad (1)$$

where $J_{S_0}(\lambda)$ is the solar spectral irradiance for air mass zero at wavelength λ and $\rho(\lambda)$ is the spectral reflectance. In order to

facilitate an experimental calculation of ρ_{S_0} , the solar energy distribution curve (ref. 8) was divided into 50 wavelength intervals so that each incremental energy interval corresponded to 2 percent of the total solar energy (fig. 4). The spectral reflectance could not be measured below 0.316 μm , nor could it be measured above 2.30 μm . Therefore, forty-seven equal energy increments (94% of total solar irradiance) were used to approximate ρ_{S_0} . The numerical approximation of equation (1) is

$$\rho_{S_0} \approx \frac{\sum_{i=1}^{i=47} \bar{\rho}_i(\lambda) (\Delta E)_i}{\sum_{i=1}^{i=47} (\Delta E)_i} = \frac{1}{47} \sum_{i=1}^{i=47} \bar{\rho}_i(\lambda) \quad (2)$$

where ΔE is an increment of solar energy flux and $\bar{\rho}_i(\lambda)$ is the average spectral reflectance over a given increment of solar energy flux.

The spectral reflectance, $\rho(\lambda)$, is determined by the ratio of the detector signal with the incident beam from the monochromator focused on the sample to the detector signal with the incident beam focused on the magnesium oxide wall of the sphere. A spectral reflectance datum point is obtained by setting the wavelength to the mean wavelength of an energy increment and setting the monochromator slit width to correspond to the energy increment wavelength range (ref. 9). Spectral absorptance $\alpha(\lambda)$, is obtained by subtracting spectral reflectance from unity.

The corresponding total solar absorptance at air mass zero, α_{S_0} is

$$\alpha_{S_0} = 1 - \rho_{S_0} \quad (3)$$

This technique has been previously used (ref. 10).

Equations (1), (2), and (3) can be applied to the calculations for the solar spectrum using air mass 2 distribution. Air mass 2 represents the solar spectrum after light passes through the atmosphere. It has absorption-bands which correspond to ozone, water, and CO_2 (ref. 11). $J_{S_2}(\lambda)$, the solar spectral irradiance weighted at air mass 2 using the same 47 wavelength intervals as $J_{S_0}(\lambda)$, was incorporated into equations (1) and (2) to obtain the total solar reflectance at air mass 2, ρ_{S_2} . ρ_{S_2} was subtracted from unity to obtain the total solar absorptance at air mass 2, α_{S_2} (eq. 3).

Optical properties of the materials in the infrared region (1 to 16 μm) were obtained using a holraum reflectometer (ref. 12). A water cooled (20 $^{\circ}\text{C}$) ion textured sample 2 cm in diameter was placed into a nickel chamber that had a nickel oxide coating and was heated to 900 $^{\circ}\text{C}$. The reflected radiation from the sample was directed into a monochromator. The monochromator was driven by an electric motor to obtain a continuous reflectance curve for the wavelength region of 1.0 μm to 16 μm . A nickel oxide sample was used as the reference sample, and a continuous reflectance curve was obtained for this sample. The spectral reflectance is the ratio of the ion textured sample reflectance at one wavelength to the nickel oxide sample reflectance at the same wavelength. Reflectance values starting at a wavelength of 1.0 μm to 16 μm (in increments of 0.5 μm) were used to obtain total emittance. The data was normalized for a 425K black body. The calculation for total emittance, ϵ_T , is

$$\epsilon_T = 1 - \frac{\int \rho(\lambda) \phi(\lambda) d\lambda}{\int \phi(\lambda) d\lambda} \approx 1 - \frac{\sum_{i=1}^{31} \rho_i(\lambda) \phi_i(\lambda) (\Delta\lambda)_i}{\sum_{i=1}^{31} \phi_i(\lambda) (\Delta\lambda)_i} \quad (4)$$

where $\rho_i(\lambda)$ is the spectral reflectance at $i = 1, 1.5, 2, \dots, 16 \mu\text{m}$
 $\phi_i(\lambda)$ is the spectral irradiance from a 425 K black body
 $(\Delta\lambda)_i$ is 0.5 μm .

RESULTS AND DISCUSSION

All five materials were ion textured by 1000 eV Xe ion beam. Each material was exposed to the ion beam for different lengths of time. The sample was textured until the surface appearance did not change and looked black by visual observations. The exposure times are given in table I. Unpublished data indicate that the exposure times can be substantially reduced without changing the desired surface texture. The resulting microstructures were unique for each material and reproducible under identical ion source conditions. Two different kinds of microstructure were obtained. Copper, silicon, and aluminum had a texture that consisted of closely spaced cones as shown in figures 5, 6, and 7, respectively. The aluminum cones are extremely thin and needle like. The peak-to-peak spacing ranges from an average value of 1 μm for silicon to 6 μm for aluminum (table I). The spectral reflectance for copper, silicon, and aluminum textured surfaces is shown in figures 8, 9, and 10, respectively. In all cases spectral reflectance in the visible region (0.4 to 0.7 μm) is less than 0.05. Because of poor detector response, spectral reflectance values between 1.4 μm and 2.1 μm are average values of the two different

detection systems. The measured reflectance values are within 70 percent of the average value in this wavelength region as indicated in each figure. Measurement uncertainties in the 1.4 to 2.1 μm wavelength region have a small effect on the total reflectance since the irradiance for a 425 K black body is small in this region (fig. 9).

Titanium and 316 stainless steel surfaces after ion texturing are composed of a field of convoluted ridges as shown by the scanning electron photomicrographs in figures 11 and 12, respectively. The average peak-to-peak spacing for both materials is 0.5 μm . Figures 13 and 14 show the spectral reflectance for titanium and stainless steel, respectively. There is a significant increase in spectral reflectance (decrease in emittance) in the infrared wavelength region when compared to the copper, silicon, and aluminum results (figs. 8 to 10). This result is consistent with the fact that the peak-to-peak spacing is significantly less than the infrared wavelength range (1-16 μm) (ref. 13). Therefore, the surface becomes more reflective. Because titanium and 316 stainless steel have smaller ϵ_T values (by a factor of 2.5) than copper, silicon, and aluminum but have α_S 's of about equal value, α_{S_0}/ϵ_T and α_{S_2}/ϵ_T are twice as great for Ti and 316 stainless steel as for Cu, Si, and Al (table II). By using the same ion beam sputtering technique, materials have been obtained which have α_{S_0}/ϵ_T or α_{S_2}/ϵ_T ratios near unity (Cu, Si, and Al) or near 3 (Ti and 316 SS).

By changing the arrival rate of the seed material used in the texturing process (refs. 3 and 4), the cone structure density can be altered and potentially result in lower values of ϵ_T for Cu, Si, and Al.

Surfaces that have a high solar absorptance are currently being considered for use as solar collectors. Though the emittance values of the ion textured materials (0.38 to 0.88) are not as low as black chrome (0.12, ref. 14), it has been shown (refs. 14 and 15) that several physical principles may be used to form selective absorbing surfaces. In a practical system the highest possible value of α_S is desirable. This principle is met by the ion textured surfaces. It is of interest to calculate the equilibrium temperature of ion textured surfaces to assess the potential use in either space or terrestrial application. The following cases were selected for such an evaluation: 1) a surface in space absorbing solar radiation and reflecting radiation from one side only, 2) a surface in space absorbing solar radiation and emitting from both sides, 3) a solar terrestrial collector for which the stagnation temperature ($T_{c,2}$) is calculated with no heat extracted from the system.

Shown in table II (case I) are the equilibrium temperatures ($T_{c,\text{space}}$) attained by each of these materials while exposed to the energy flux of one sun ($140\text{mw}/\text{cm}^2$) in space and omitting from the front surface only. The Ti and 316 stainless steel surfaces reached the highest temperature levels, since these surfaces had the highest α_S/ϵ_T ratio. For all the calculations, the emittance was normalized to a blackbody at 425 K as shown in equation (4).

Also presented in table II (case II) are the equilibrium temperatures which each of these materials would reach if there were front surface absorption and emission from both surfaces. This type of collector can be utilized where photo-thermal conversion of solar energy is desirable, at collector temperatures less than 425 K (ref. 15). Here the photo-thermal collector absorbs the energy of the sun and then acts as a radiator for infrared radiation at the collector operating temperature. Thus, for this type of collector all the textured surfaces have the correct optical properties that result in temperature levels of less than 425 K. Cu, Si, and Al as a front surface radiator only, also reach values less than 425 K in space.

For terrestrial applications the solar absorptance values ($\alpha_{S,2}$) calculated for air mass 2 are shown in table II. In spite of the absorptance bands in the atmosphere for air mass 2, there is only a 1 percent difference between the absorptance at air mass zero and the absorptance calculated for air mass 2 for all five ion textured metals.

Shown in table II (case III) are calculated values of the temperature of a collector, $T_{c,2}$, having a glass surface placed over it and a vacuum between the two surfaces. For this case there are no convective losses (reflections which are small are also neglected) and no heat is extracted from the collector. Thus the stagnation temperature ($T_{c,2}$) can be calculated for each textured surface from a heat balance equation which is shown to be:

$$\tau_1 \alpha_c \phi = \frac{\alpha_g \sigma (T_{c,2}^4 - T_g^4)}{\left(\frac{1}{\epsilon_g} + \frac{1}{\epsilon_T} - 1 \right)} + \epsilon_g \sigma (T_g^4 - T_{sky}^4) \quad (5)$$

where τ_1 = transmittance of glass (0.97)
 α_c = collector absorptance
 ϕ^c = solar flux, 100 mw/cm²
 α_g = absorptance of glass = 0.9
 ϵ_g = emittance of glass = 0.9 at 310 K
 σ^g = 5.67×10^{-5} erg/sec cm² K = 5.67×10^{-5} watts/cm² K
 T = glass temperature
 T_{sky} = sky temperature
 ϵ_T = collector emittance
 $T_{c,2}$ = collector stagnation temperature

In this equation the left side is the radiation absorbed by the collector. The first term on the right side of equation (5) is the radiation emitted by the collector and absorbed by the glass cover. The

second term on the right side is the heat radiated by the glass cover to the sky. Equation (5) can be put in the form

$$T_{c,2}^4 = \frac{\tau_1 \alpha_c \phi}{\alpha_g \sigma} \left(\frac{1}{\epsilon_T} + \frac{1}{\epsilon_g} - 1 \right) - \left(\frac{1}{\epsilon_T} + \frac{1}{\epsilon_g} - 2 \right) T_g^4 + \left(\frac{1}{\epsilon_c} + \frac{1}{\epsilon_g} - 1 \right) T_{sky}^4 \quad (6)$$

For ease of calculation a value of 310 K was set for the glass cover to conform with that of the collector systems of references 14 and 16. (Varying T_g by 30 K changes $T_{c,2}$ by 10 K). Collector stagnation temperature values of the ion textured surfaces ($T_{c,2}$) are shown in the last column of table II. For Ti and 316 stainless steel the highest values of collector temperatures were obtained, 459 K and 468 K, respectively. These values are slightly less than a black chrome collector system (505 K stagnation temperature, ref. 16). However, the upper limit stagnation temperature levels are important from a safety consideration because of the building materials involved. (Fiberglass insulation with a bakelite binder was used to construct the solar collector of ref. 16). For this system Cu, Si, and Al ion textured surfaces could be utilized.

The present data of the ion textured surfaces probably do not yield a favorable efficiency/cost trade relative to electroplated coatings. Ion textured emissivities are relatively high for use as solar collection surfaces and surface processing may be quite expensive. However, because the surface roughness material is an integral part of the substrate and not plated or painted onto it, ion textured surfaces may potentially be more durable than present coatings. The only potential means of degradation with time is through alterations of the surface texture. Therefore, these surfaces may be far more durable than present coatings. Additional system studies (cost/efficiency and reliability) might be made for a system using ion textured aluminum foil. The aluminum surface structure might be optimized to smaller dimensions which would yield lower processing time, lower cost, and potentially a lower emissivity.

CONCLUSIONS

Ion beam textured, cone-like surfaces were developed on copper, silicon, and aluminum. Each material has a unique microstructure which is reproducible under the identical ion source conditions. The peak-to-peak spacing between the resulting surface cones ranged from 1 μm for silicon to 6 μm for aluminum. These microstructures resulted in α_s values greater than 0.95 for air mass zero and 2 and ϵ_T values between 0.77 and 0.86 normalized for a 425 K black body.

Titanium and 316 stainless steel developed serpentine ridge microstructures when exposed to 1000 eV He ion beam. The average peak-to-peak distance was 0.5 μm for both materials. The calculated α_{S_1} and α_{S_2} values for titanium were both 0.96 and for 316 stainless steel were 0.93 and 0.94, respectively. ϵ_T was 0.43 for titanium and 0.38 for 316 stainless steel when normalized to a 425 K black body.

Calculations using the experimental values of α_S and ϵ_T for each material indicate that selective absorbing surfaces with stagnation temperatures ranging from 409 K for Cu to 494 K for 316 stainless steel can be obtained. A black chrome collector with a solar collection system would yield a stagnation temperature of 505 K.

Ion textured surfaces may degrade very little with time resulting in low maintenance costs although the initial processing costs may be higher than the costs of presently used coatings. Refinements in the ion texturing process for each individual material may result in durable surfaces with better optical properties (higher absorptance and lower emittance) for solar collection.

REFERENCES

1. J. Jurisson, R. E. Peterson, and H. Y. B. Mar, J. Vac. Sci. Technol. 12, 1010 (1975).
2. R. S. Berg and G. J. Kominiak, J. Vac. Sci. Technol. 13, 403 (1976).
3. G. K. Wehner and D. J. Hajicek, J. Appl. Phys. 42, 1145 (1971).
4. W. R. Hudson, Ion Beam Texturing, presented at the 23rd American Vacuum Society Meeting, Chicago (1976).
5. W. R. Hudson and B. A. Banks, AIAA Paper. 75-425, New Orleans, La. (1975).
6. J. R. Beattie and P. J. Wilbur, AIAA Paper 75-429, New Orleans, La. (1975).
7. D. K. Edwards, et al., J. Opt. Soc. Am. 51, 1279 (1961).
8. NASA SP-8005 (1965).
9. Introduction to Infrared Spectroscopy, Vol. 1, Perkin-Elmer Corp. (1952).

10. E. W. Spisz, et al., NASA TN D-5353 (1969).
11. H. Brandhorst, et al., NASA TM X-71771 (1975).
12. M. J. Mixtich and H. Mark, NASA TN D-3187 (1966).
13. R. E. Peterson and J. W. Ramsey, J. Vac. Sci. Technol. 12, 174-181 (1975).
14. G. E. McDonald and H. B. Curtis, NASA TM X-71731, (1975).
15. D. M. Mattox, J. Vac. Sci. Technol. 13, 127 (1976).
16. J. W. Ramsey, J. T. Borzoni, T. H. Holland, Development of Flat-Plate Solar Collectors For the Heating and Cooling of Buildings, Honeywell, Inc. Report HONEYWELL-2852-40057 (1975). Also NASA CR-134804.

TABLE I. - ION TEXTURED SURFACE PARAMETERS
OF Cu, Si, Al, Ti, AND 316 STAINLESS STEEL

Material	Ion beam sputtering duration at 1 kv and 100 ma (min)	Type of structure	Peak to peak μm	Height μm	Surface structure growth rate $\mu\text{m}/\text{min} \times 10^{-4}$
Copper	90	cone	3	4.4	490
Silicon	240	cone	1	0.9	38
Aluminum	270	cone	6	15.2	560
Titanium	447	ridge	0.5	0.3	6.7
316 Stainless steel	540	ridge	0.5	0.5	9.3

TABLE II. - OPTICAL PROPERTIES OF ION TEXTURED SURFACES

Material	Air mass zero							Air mass two		
	ρ_S (0.33-2.6) μm	$\alpha_{S,0}$	$\rho_{\text{I.R.}}$ 1.5-15.5	ϵ_T 425 K B.B.	$\alpha_{S,0}$ ϵ_T	$T_{t,\text{space}}$		$\alpha_{S,2}$	$\alpha_{S,2}$ ϵ_T	$T_{c,2}$ glass cover at 310 K Case III K
						$\alpha_{S,0}$ ϵ_T	$\alpha_{S,0}$ $2\epsilon_T$			
						Case I K	Case II K			
Copper	0.055	0.945	0.154	0.864	1.09	404	342	0.957	1.11	410
Silicon	.027	.973	.249	.776	1.25	419	352	.976	1.26	416
Aluminum	.028	.972	.195	.822	1.18	413	347	.972	1.18	412
Titanium	.043	.957	.633	.434	2.21	482	405	.966	2.23	459
316 Stainless steel	.073	.927	.678	.382	2.43	494	415	.941	2.46	468

REPRODUCIBILITY OF THE ORIGINAL PAGE IS POOR

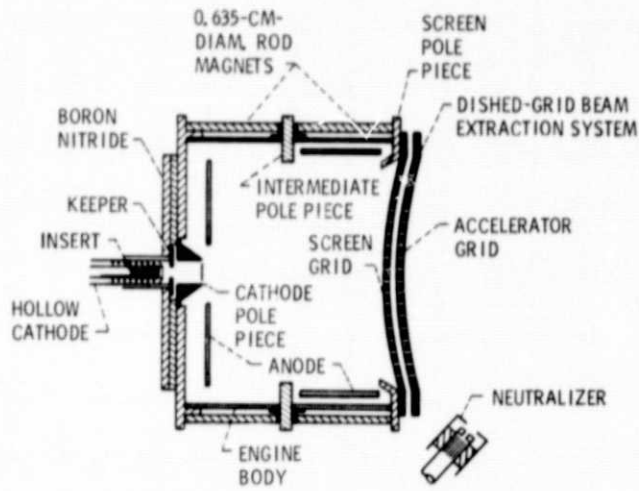


Figure 1. - Xenon ion beam source. Cross-sectional view.

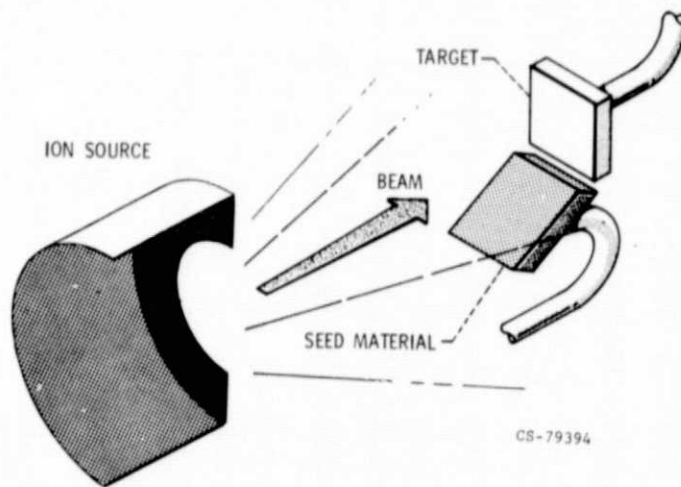


Figure 2. - Sketch of the apparatus arrangement used for ion beam texturing.

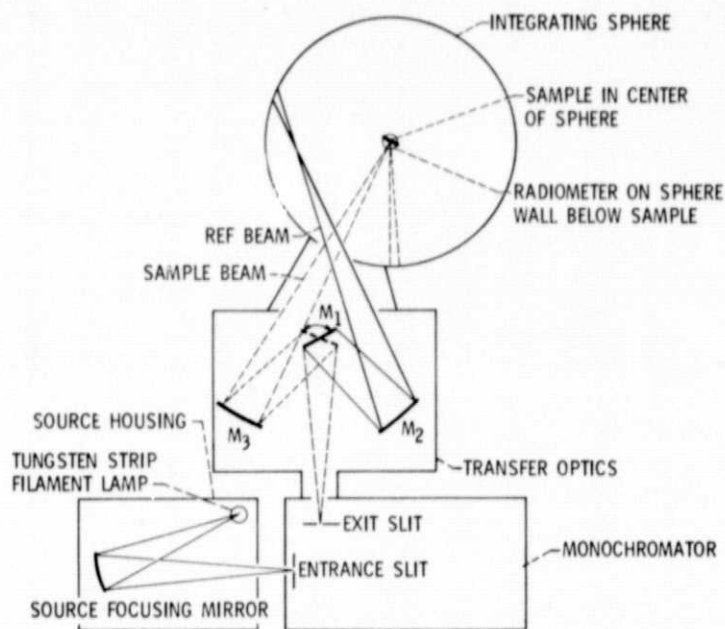


Figure 3. - Experimental arrangement for integrating sphere reflectometer.

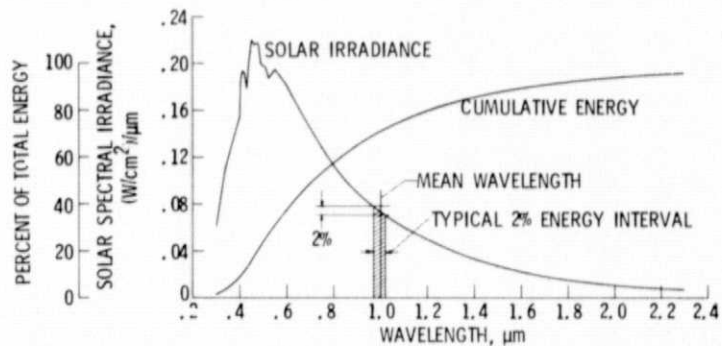


Figure 4. - Solar energy distribution curve.

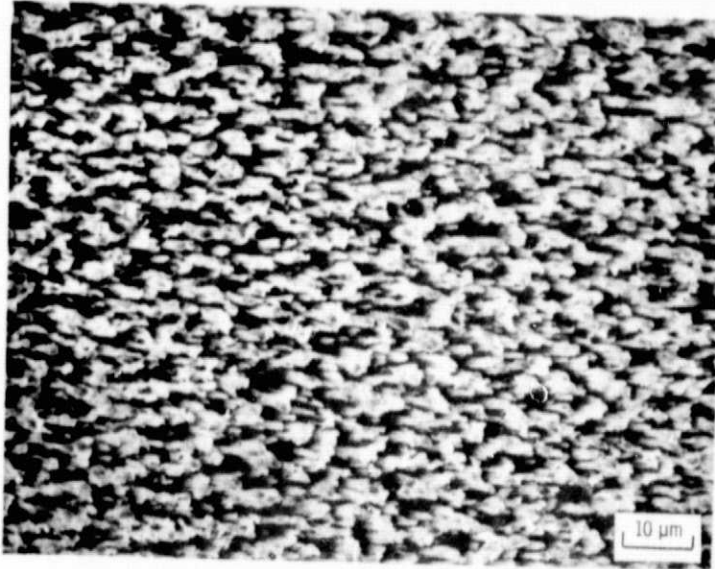


Figure 5. - Scanning electron photomicrograph of an ion beam textured copper surface.

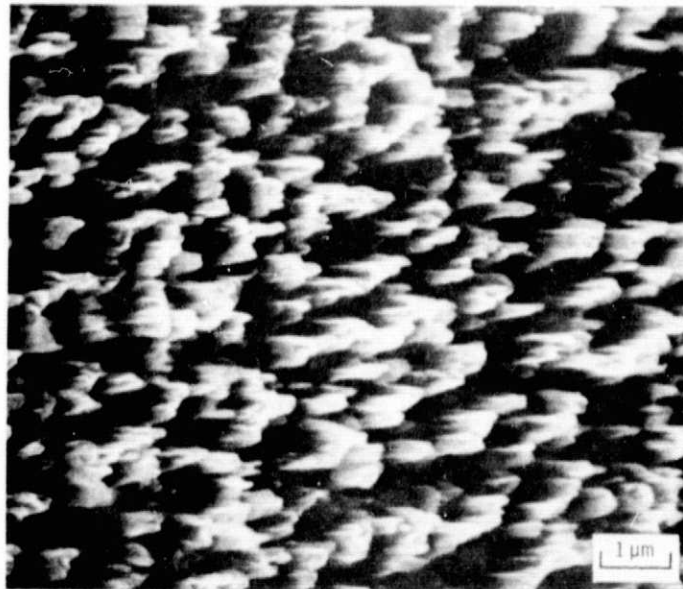


Figure 6. - Scanning electron photomicrograph of an ion beam textured silicon surface.

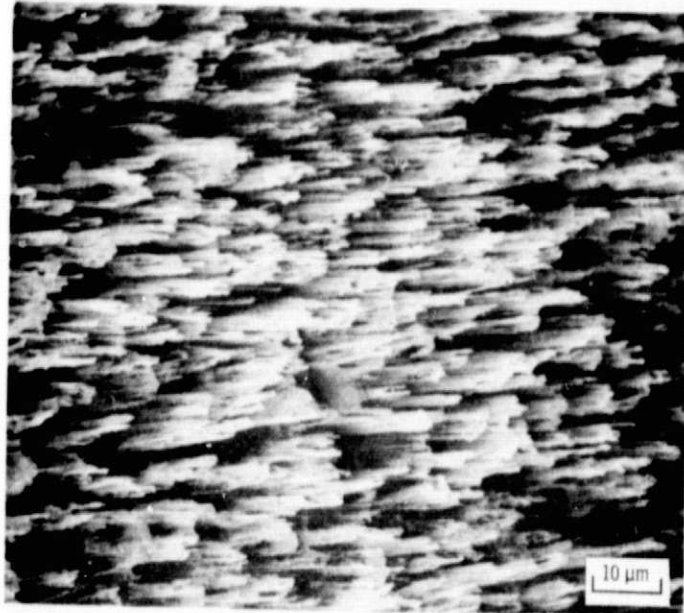


Figure 7. - Scanning electron photomicrograph of an ion beam textured aluminum surface.

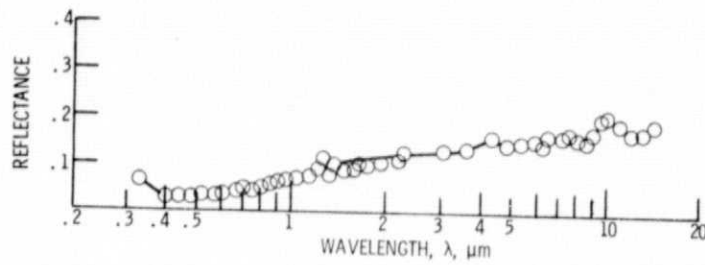


Figure 8. - Spectral reflectance for ion beam textured copper.

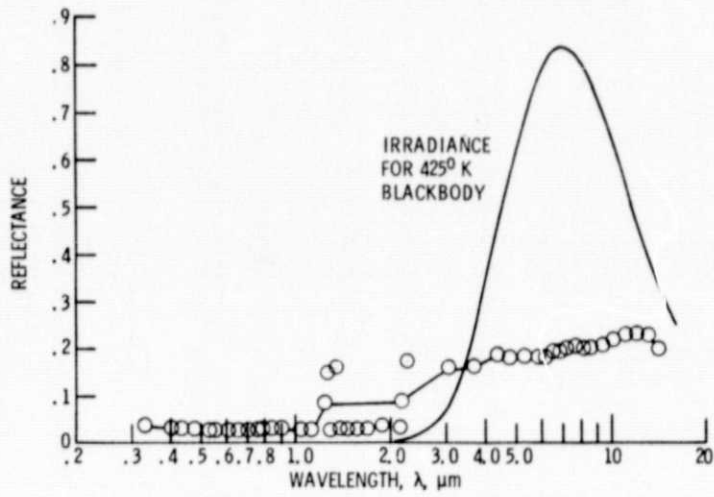


Figure 9. - Spectral reflectance for ion beam textured silicon.

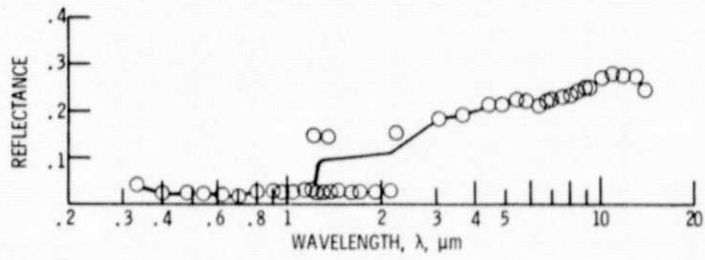


Figure 10. - Spectral reflectance for ion beam textured aluminum.

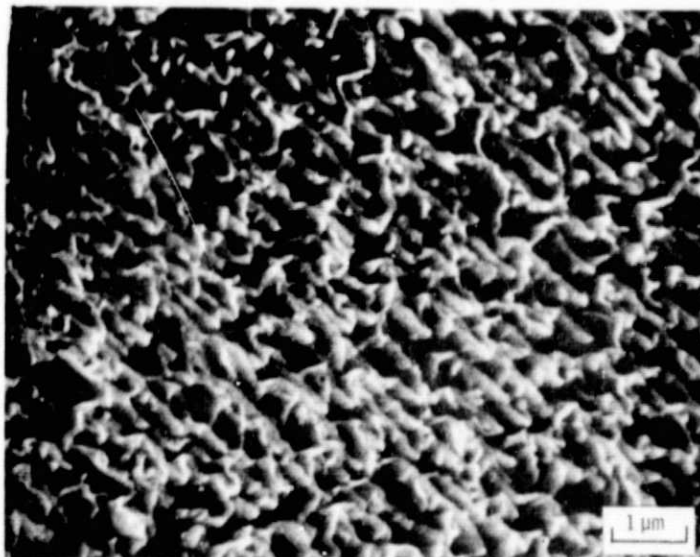


Figure 11. - Scanning electron photomicrograph of an ion beam textured titanium surface.

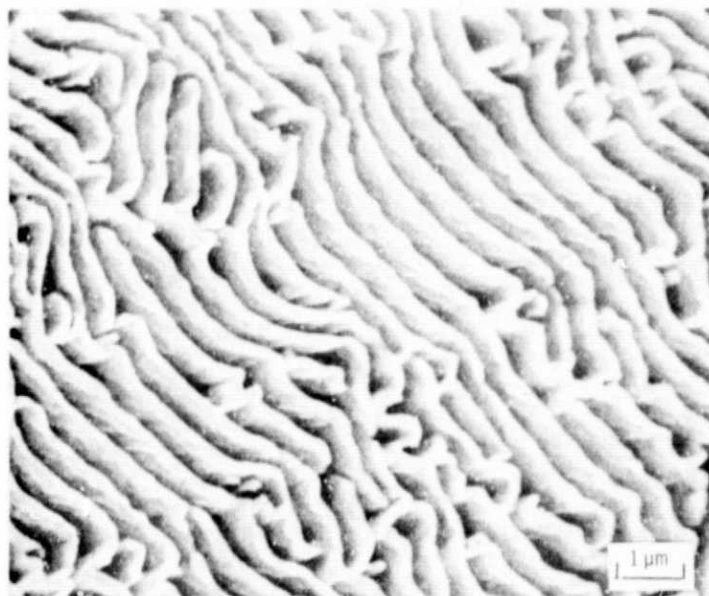


Figure 12. - Scanning electron photomicrograph of an ion beam textured stainless steel surface.

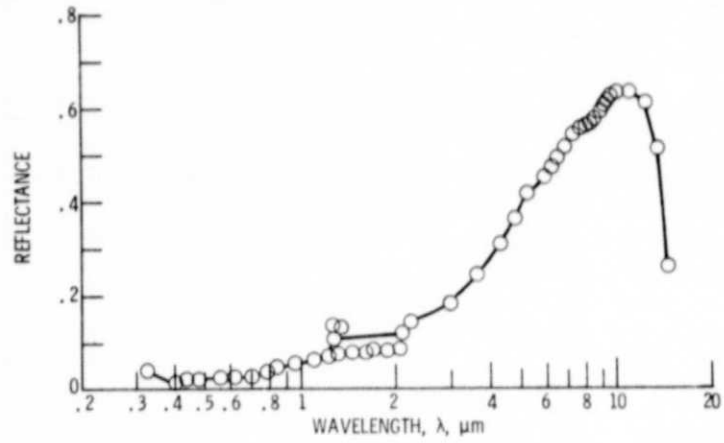


Figure 13. - Spectral reflectance for ion beam textured titanium.

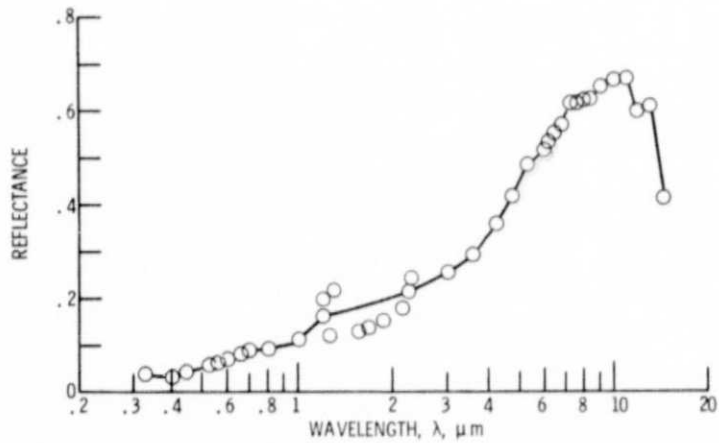


Figure 14. - Spectral reflectance for ion beam textured 316 stainless steel.